Experimental Thermal and Fluid Science 44 (2013) 161–173

Contents lists available at SciVerse ScienceDirect

Experimental Thermal and Fluid Science

journal homepage: www.elsevier.com/locate/etfs

Measurement of heat flux in dense air-mist cooling: Part II – The influence of mist characteristics on steady-state heat transfer

Constantin A. Hernández-Bocanegra [a,1], Jesús I. Minchaca-Mojica [a,1], A. Humberto Castillejos E. [a,*], Francisco A. Acosta-González [a,1], Xiaoxu Zhou [b,2,3], Brian G. Thomas [b,2]

[a] Department of Metallurgical Engineering, Centre for Research and Advanced Studies, CINVESTAV – Unidad Saltillo, Carr. Saltillo-Monterrey Km. 13.5, Ramos Arizpe, Coahuila 25900, Mexico
[b] Department of Mechanical Science and Engineering, University of Illinois at Urbana-Champaign, 1206 West Green Street, Urbana, IL 61801, USA

ARTICLE INFO

Article history:
Received 28 June 2011
Received in revised form 21 February 2012
Accepted 5 June 2012
Available online 19 June 2012

Keywords:
Spray cooling
Steady-state heat flux measurement
Spray characteristics
Stable film boiling regime
Heat flux correlation
Steel continuous casting

ABSTRACT

The boiling convection heat flux, $-q$, taking place during the impingement of a water air-mist upon the surface of a Pt-disk, held at steady-state surface temperatures T_w ranging between 550 and 1200 °C, has been measured under different conditions of water impact density, w, droplet velocity, u, and droplet size, d_d. The new steady-state measurement method controls induction heating to balance the heat extracted from the sample, as described in detail in Part I. Local mist characteristics were determined at room temperature in free non-impinging mists using a patternator for w and a particle/droplet image analyzer (PDIA) for d_d and u at positions equivalent to those of the Pt-disk. Three different air-mist nozzles of fan discharge type are characterized over their full range of water flow rates and air inlet pressures and using different positions of the hot surface with respect to the nozzle, to cover the following ranges of local spray characteristics: w from 2 to 106 L/m^2 s; normal volume weighted mean velocities, $u_{z,v}$, from 9.3 to 45.8 m/s and volume mean diameters, d_{30}, from 19 to 119 μm. Increasing the air nozzle pressure at constant water flow rate generates mists with finer and faster drops that lead to a higher frequency of drops with large impinging Weber numbers, suggesting a higher probability of wet contact with the surface and an enhanced heat extraction. Heat fluxes as large as ~12 and ~10 MW/m^2 were found in the transition and stable film boiling regimes, respectively. The boiling convection heat flux in the range of 750–1200 °C, which corresponded to stable film boiling, was found to correlate very well with the mist characteristics and temperature. The order of importance of the four parameters influencing $-q$ was: $d_{30} \ll T_w < w \approx u_{z,v}$. For given local water flux and surface temperature, the correlation indicates that spray cooling becomes more intense as the velocity of the drops increases; the droplet size plays a very minor role. Compared with previous results using a transient method, the steady-state heat transfer coefficients increase faster with w in the range of 5–20 L/m^2 s, reaching much higher values. This suggests that within this range, the steady-state heat flux is controlled by the local water flux, while the transient heat flux must be controlled by the supply of heat conducted to the surface.

1. Introduction

As mentioned in Part I of this two-part article [1], the use of sprays is ubiquitous in cooling processes for many diverse applications and the complex nature of heat transfer during spraying plays a critical role for success in all of them. The importance of spray cooling in steel continuous casting is easily realized by considering that in 2011, the annual world crude steel production reached 1515 m tons [2], while the proportion of continuously cast steel must be higher than 92%. Recognizing that spray/air-mist cooling is essential to both the quality and productivity of this process, its great relevance is clearly evident. In continuous casting, the solidified shell leaves the mold or primary cooling system with a surface temperature $T_w \sim 1050$ °C. Then, the solidifying strand continues its way through cooling zones formed by a series of alternating containment rolls and spray cooling nozzles that comprise what is called the secondary cooling system; where the maximum and minimum surface temperatures are ~1200 and

* Corresponding author. Tel.: +52 844 438 9600x8666; fax: +52 844 438 9600.
E-mail addresses: constantin.hernandez@cinvestav.edu.mx (C.A. Hernández-Bocanegra), jesus.minchaca@cinvestav.edu.mx (J.I. Minchaca-Mujica), humberto.castillejos@cinvestav.edu.mx (A. Humberto Castillejos E.), andres.acosta@cinvestav.edu.mx (F.A. Acosta-González), xzhou9@uiuc.edu, xiaoxu.zhou@ssab.com (X. Zhou), bgthomas@uiuc.edu (B.G. Thomas).
[1] Tel.: +52 844 438 9600x8666; fax: +52 844 438 9600.
[2] Tel.: +1 217 333 6919; fax: +1 217 244 6534.
[3] Present address: Research & Development Department, SSAB Iowa Inc., 1755 Bill Sharp Blvd., Muscatine, IA 52761, USA.

0894-1777/$ - see front matter © 2012 Elsevier Inc. All rights reserved.
http://dx.doi.org/10.1016/j.expthermflusci.2012.06.007

Nomenclature

a	cross section area of collector tubes in patternator (m^2)
A	air flow rate in the nozzle at 273 K and 1 atm (NL/s)
CHF	critical heat flux (MW/m^2)
d_d, d_{30}, d_{32}	drop diameter; volume mean diameter; Sauter mean diameter (μm)
E_k	kinetic energy flux of droplets (W/m^2)
h	heat transfer coefficient for boiling convection ($kW/m^2\,K$)
n	droplet number density (m^{-3});
$\dot{N}$	droplet number flux ($m^{-2}\,s^{-1}$)
N	total number of droplets i in a sample
p_a, p_w	manometric air-atomizing; water inlet pressures (kPa)
$-q$, $-q_c$	boiling convection; combined heat flux (MW/m^2)
t	time for water collection in patternator (s)
T_f, T_L, T_w, T_∞	water; Leidenfrost; surface and surrounding temperatures (°C)
u, u_x, u_z	magnitude of velocity; tangential; normal velocity components of individual drops at virtual impingement position (m/s)
u_{10}	arithmetic mean velocity (m/s)
u_v, $u_{x,v}$, $u_{z,v}$	volume weighted mean of velocity magnitude; of x-velocity; of z-velocity component (m/s)
v	volume of water collected in a given tube in patternator (L)
w	local water impact density (or flux) ($L/m^2\,s$)
W, W_c	measured; calculated total water flow rates (L/s)
We_{zs}	impingement Weber number
x, y, z	rectangular coordinates with origin at center of nozzle orifice (m)
z_s	setback distance of nozzle exit from impingement surface (m)

Greek

α	main expansion angle of mist jet (°)
ε	emissivity
ρ_d	density of liquid (kg/m^3)
θ	angle between z-axis and line connecting the center of nozzle orifice with the center of a given collecting tube entrance (radians)
σ, σ_r	surface tension of liquid ($kg\,s^{-2}$); Stefan–Boltzmann constant, 5.669×10^{-8} ($W/m^2\,K^4$)

Subindex

i	integer denoting a drop in a sample

750 °C, respectively. The cooling in this system should entirely solidify the strand, without generating internal or surface defects. But, this will depend on the cooling conditions. Heat is extracted in the secondary cooling system by different mechanisms: direct spray impingement, conduction by roll contact, radiation and boiling convection to draining water [3]. Of these, spray cooling accounts for ~60% of the total heat extracted, and its share can be much larger in the first zones of the secondary cooling system [4,5]. Thus, there is a great incentive to understand how the spraying conditions should be selected and controlled to optimize the intensity and uniformity of heat extraction. For the surface temperatures prevailing in steel secondary cooling, direct spray heat transfer may occur in the regimes of stable film boiling and transition boiling. A large number of investigations have been carried out to study these regimes using different approaches [6–8,15,18–20,23–28].

Single droplet streams have been used to determine the effect of the droplet characteristics on heat transfer in the film boiling regime [6,7]. Pedersen [6] used droplet diameters d_d between 100 and 500 μm and velocities u between 3 and 9 m/s to represent those found in spray cooling and used droplet frequencies between 40 and 100 s^{-1} to minimize the hydrodynamic and thermal interference caused by interaction between successive droplets. Increasing the velocity at impingement significantly increased the heat transfer rate within the stable film boiling regime, but the surface temperature was found to have little effect. Droplets with small diameters were observed to exhibit similar deformation and break-up behavior as the larger droplets (~2000 μm Ø) studied by Wachters and Westerling [8]. Hence, for both large and small drops, the impingement Weber number ($We_{zs} = \rho_d u_z^2 d_d/\sigma$) based on the collision velocity normal to the surface, u_z, has been commonly used to characterize the impact behavior. Several different impact behaviors for $T_w = 400$ °C were observed [8]: (a) for $We_{zs} \leqslant 30$, a drop impinging on a surface spread and then recoiled before the whole drop rebounded elastically from the surface; (b) for $30 < We_{zs} < 80$, the drop underwent disintegration only after starting to rebound inelastically from the surface; and (c) for $We_{zs} \geqslant 80$, the drop began to disintegrate during the initial part of the collision to form a thin liquid film that spread over the surface. These classical results for a single surface temperature have been extended to map qualitatively the drop impingement outcomes or behaviors in terms of We_{zs} and T_w, since reliable data describing the transition between the several regimes are unavailable [9]. As pointed out by Moreira et al. [10] different impact behaviors occur within different boiling heat transfer regimes, and the temperature ranges of the boiling regimes depend on the impact conditions [11]. Additionally, Panão and Moreira [12] have indicated that the prediction of spray impact regimes based on drop characteristics obtained from measuring free, non-impinging sprays may be quite different from those estimated using two phase flow parameters measured in the presence of the target impacting surface. This would be expected since the velocity and size of the primary droplets are affected by the change in the direction of motion of the air in the vicinity of the target surface and by their interaction with secondary droplets splashed from the liquid film formed by preceding drops. In a study involving high-speed diesel sprays, Park and Lee [13] reported that the effect of impingement is negligible at 10 mm separated from the wall and showed that the properties of drops in impinged sprays are related to those in free sprays.

The identification of the impact regimes is complicated due to the difficulties in visualizing or detecting the phenomena taking place in the surface. Bernardin et al. [14] had to complement visual observations of the impingement phenomena with an electrical contact technique to identify that in the film boiling regime, with a $T_w = 280$ °C, even droplets with small We_{zs} (=20) were able to establish wet contact during some of the drop spreading time. It has been reported [15] that with the increase in the We_{zs} the drop heat extraction effectiveness increased in both the transition and film boiling regions as a result of a more intimate contact of the drop with the surface. The heat extraction effectiveness is defined as the ratio of the actual heat extracted by the drop to the maximum possible heat extracted due to the latent and sensible heats involved in generating superheated vapor at T_w from the drop. Different from Pedersen [6], Bernardin and Mudawar [7] found that in the film boiling regime the heat transfer rate augmented

considerably with the increase in surface temperature and droplet size and much less with droplet velocity. The main difference between the two studies was the much larger droplet frequency used in [7], from ~400 to ~12000 s^{-1}. These large droplet frequencies may have also caused that in contrast to the results reported by Issa and Yao [15] the heat transfer effectiveness was found to vary inversely with the droplet velocity. Recent works by Moreira et al. [10] and Moreira and Panão [11] on fuel sprays impinging onto hot surfaces show that the interaction between drops modifies the heat extraction phenomena. They point out that the accuracy of the empirical correlations for spray heat transfer strongly depends on the experimental conditions.

Sprays and air-mist are dispersions of drops produced by single-fluid (e.g. water) and twin-fluid (e.g. water–air) nozzles, respectively; also referred to as hydraulic and pneumatic nozzles, respectively. In sprays, the energy to fragment the water into moving drops is provided by the pressure drop generated across the narrow nozzle exit port and in air-mists, a high speed air-stream breaks a water stream into fine, fast-moving droplets [16,17]. In both cases, the resulting droplet system consists of a wide spectrum of drop sizes, drop velocities, and water fluxes. Additionally, these parameters do not vary independently, so the study of their individual effects on heat extraction is complicated. Therefore, some nozzles have been designed to generate mono-disperse sprays, where d_d, u and w are unique or exhibit narrow distributions and also can be controlled independently [18,19]. In a study with mono-dispersed sprays, Choi and Yao [18] claimed that for horizontally impacting dilute sprays, the heat flux in the film boiling regime (between 250 and 500 °C) increased with increasing w, d_d, or u, while no effect of d_d or u was observed for dense sprays. It was claimed that this was a result of interference between successive droplets. In their investigation w varied in the range of 0.11–1.84 L/m^2 s, d_d was equal to 430 and 560 μm and u was 3.2 and 4.2 m/s. Celata et al. [19] developed a mono-dispersed spray device that generated drops with the following property values: d_d = 150, 300, 450 and 900 μm and u = 2,3,4,5,6 and 7 m/s. In their study, it was found that heat transfer from a vertical surface, as indicated by the rewetting velocity, was affected by the droplet diameter and velocity for T_w < 500 °C, but not at higher temperatures.

As accounted by Brimacombe et al. [20], the boiling convection heat flux, $-q$, of hydraulic commercial nozzles has been found by many investigators to depend on water impact flux, w, in the stable film boiling regime. But, the $-q$ values reported were different among different nozzles for the same w, hinting that other spray parameters influenced by the nozzle type and operating conditions affected the heat flux. Also, in a study concerning the nucleate boiling regime, Chen et al. [21] presented different critical heat fluxes for different nozzles but the same w. An analogous behavior was reported by Ciofalo et al. [22] for the heat transfer coefficient during spray cooling in the single phase convection regime. These results along different regimes of the boiling curve indicate the dependence of the heat extraction on parameters other than simply the water impact flux. These other parameters are: ensemble averages of droplet size, droplet velocity, droplet number density, n, and droplet number flux, $\dot{N}$. Chen et al. [21] selected the Sauter mean diameter, d_{32}, and the arithmetic mean velocity, u_{10}, as the characteristic size and velocity averages and related the spray parameters through the following two expressions,

$$w \approx \pi d_{32}^3 u_{10} n/6; \quad \dot{N} \approx u_{10} n \tag{1a; 1b}$$

The volume conservation Eq. (1a) is satisfied when the size and/or velocity of the drops in the spray causes a corresponding change in n (or equivalently in $\dot{N}$) according to Eq. (1b). In hydraulic nozzles, the local spray characteristics at a given position are tied to the water flow rate, W, while in air-mist nozzles, the mist characteristics can change for the same W by varying the air inlet pressure, p_a. In 'conventional' commercial hydraulic and pneumatic nozzles, the spray parameters cannot be varied independently from one another, thus two approaches have been followed to study their individual effects on spray cooling. In one of them, systematic independent variation of the spray characteristics have been achieved using different nozzles, operating conditions and measuring locations, to classify the results and find monotonic variations of each chosen parameter while the other two remain nearly constant [21,23]. Following this approach and using a hydraulic nozzle, Schmidt and Boye [23] found that the droplet velocity had a significant effect on the heat transfer coefficient at constant w, while the droplet size had no effect. In their experiments, cooling took place in the stable film boiling regime under the following conditions: w from 0.16 to 0.50 L/m^2 s, u_{10} from 5 to 7 m/s, d_{30} from 30 to 110 μm and T_w from 300 to 600 °C.

In the second approach, the dependence of heat transfer parameters on spray characteristics has been determined through least-square best fitting of lumped measurements to obtain power law expressions. Fujimoto et al. [24] presented the following expression for the heat transfer coefficient h in the stable film boiling regime, in terms of the volume mean diameter, d_{30}, volume weighted mean velocity, u_v, and water impact density, w,

$$h = 2.89 w^{0.65} u_v^{0.45} d_{30}^{-0.85} \tag{2}$$

The exponents in this expression indicate that all three spray parameters had a significant effect on h, within the following range of conditions: d_{30} from 63 to 206 μm, u_v from 6.8 to 15.6 m/s and w from 0.25 to 2.18 L/m^2 s. From a plot reported [17] for the heat transfer coefficient versus the kinetic energy flux, E_k, in the stable film boiling regime, the following expression was derived,

$$h = 118.03 E_k^{0.277} = 118.03 (\rho_d w)^{0.277} u_{10}^{0.554} \tag{3}$$

where ρ_d is the density of the liquid. For Eq. (3) the range of applicable conditions included d_{32} and u_{10} of 125–520 μm and 0.2–20.8 m/s, respectively, but the range for w was not specified. In other studies [25–28] involving air-mist nozzles the increase in p_a at constant W has been found to cause the increase in the boiling convection heat flux as a result of changes in the spray parameters, but no correlations were established between these parameters and h. It should be noticed that the drop size and velocity used to interpret the heat transfer results in the investigations cited [17–19,21–24] were determined in the absence of a hot surface, i.e., they were measured for non-impinging free sprays, at positions where the target would be placed in the thermal measurements. Recently, Panão and Moreira [29] measured simultaneously the spray droplet characteristics and the thermal behavior of an impinged wall to derive empirical correlations for the heat transfer taking place during intermittent spray impingement. Specifically, a thermal management fluid (HFE-7100, which boils at 61 °C) was impinged onto an aluminum target at T_w between 81 and 131 °C. Adequate consideration of the dynamics of intermittent sprays was emphasized as important to improve the accuracy of heat transfer correlations.

From this literature review, it is apparent that only sparse information exists on the heat transfer from a metal surface at temperatures between 550 and 1200 °C, especially for mist cooling under intense spraying conditions, for w from 2 to 106 L/m^2 s. Hence, the objective of the present work was to accurately quantify the effect of the mist parameters: w, d_d, and u, on the heat $-q$ extracted at high temperatures and under steady-state conditions, using typical commercial air-mist nozzles. The first step is measurement of the heat flux using the steady-state technique described in Part I, where the temperature field in a Pt-sample is held constant by balancing the heat extracted with the heat supplied by induction heating. The second step is measurement of the mist/droplet

properties along the major axis of the free, non-impinging mist where the Pt-sample would stand in the thermal experiments (referred to as 'virtual impact plane' from hereon). A patternator was used for w and a particle/droplet image analyzer (PDIA) for the distribution of d_d and u. A correlation was developed to predict $-q$ as a function of w, $u_{z,v}$, T_w and d_{30} in the film boiling regime, which occurs between 750 and 1200 °C. In this regime, heat fluxes as large as 10 MW/m^2 were measured. It was found that with pneumatic nozzles, the increase in air nozzle pressure at constant water flow rate generates mists with finer and faster drops that lead to a higher frequency of drops with large impinging Weber numbers. This suggests that the more intense cooling conditions obtained as p_a increases are the result of a higher probability of wet contact of the drops with the surface. For the first time, steady-state heat flux measurements under conditions of intense heat extraction are available, so it was important to compare with transient measurements reported in the literature [26].

2. Heat flux experimental method and conditions

Heat fluxes were determined using the new steady-state induction-heating-based technique described in Part I of this article [1]. In this method, a local region of an air-mist impinges horizontally upon the active surface of a Pt-disk (8 mm Ø by 2.5 mm thickness) while it is heated by induction to balance exactly its total heat losses. In this open thermodynamic system, the impinging droplets form a fluctuating liquid film on the disk surface, escape as secondary droplets, or vaporize. The Pt-disk, its surrounding induction coil and the cast ceramic monolith that embeds them comprise the measuring probe, as illustrated in Fig. 1a. Further protection from the spray was provided by placing a Plexiglas tube and a quartz cap around and in front of the ceramic, respectively. This shielded the Pt sample from any boiling heat extraction from its lateral and back surfaces. The coil is connected to a 5 kW high-frequency generator interfaced to a digital controller programmed to adjust the output power to maintain the temperature of the R-type thermocouple welded to the back of the Pt-sample at the desired set-point. The root mean square (RMS) current flowing through the coil was measured and input into a coupled inverse model of two-dimensional axisymmetric electromagnetic field and heat conduction to compute the combined heat flux, q_c, from the active surface of the sample:

$$-q_c = -q + \sigma_r \varepsilon (T_w^4 - T_\infty^4) \tag{4}$$

where $-q_c$ is made of a boiling convection, $-q$ (=$h(T_w - T_f)$) and a radiation term. In this analysis, h is the boiling convection heat transfer coefficient, σ_r the Stefan–Boltzmann constant, ε the surface emissivity and T_f, T_w and T_∞ are the water, wall and surrounding temperatures, respectively. The RMS current was measured with the high frequency ammeter illustrated in Fig. 1a.

In the experiments for each cooling condition, the temperature set-point for the sample was varied from 600 to 1200 °C in steps of 100 °C. At each temperature step, the sample was held for ~480 s, to ensure that the control temperature and the coil RMS current reached steady values. The average of these values recorded over the last 120 s of each step were used to calculate $-q_c$, $-q$ and T_w. Two different temperature paths were used: (a) the loop going from 600–1200–600 °C and (b) the descending path going from 1200 to 600 °C. About half of the experiments were carried out using each path, to verify that the heat flux was independent of the thermal history of the measuring probe in this temperature range. Each test condition was repeated at least twice and whenever a new probe was used, a previous test was repeated to verify consistent functioning of the measuring system.

Three internal-mixing air-mist nozzles with fan-shaped discharge profiles were studied: (a) W19822 (Delavan Inc., Monroe, NC), (b) Casterjet 1/2-6.5-90 and (c) Casterjet 1/2-5-60 (Spraying Systems Co., Chicago, IL); a schematic of the nozzles is displayed in Fig. 1a. Note from Table 1 that the first two nozzles deliver a mist jet with a main expansion angle $\alpha = 90°$, while the third one produces an $\alpha = 60°$. As shown in Fig. 1a for the thermal experiments, the nozzle was oriented horizontally and the axial separation z_s from the nozzle orifice to the hot surface was set according to standard commercial practices for the particular nozzle, and are listed in Table 1. The position of the probe relative to the nozzle axis was varied across the major axis x of the mist footprint, i.e., along the axis located at $y = 0$ and $z = z_s$, as specified also in table. As indicated in Fig. 1 the origin of the coordinate system is placed at the center of the nozzle tip. Further details on the thermal measurement apparatus and analysis method can be found in Part I [1].

The measured relationships between the flow rates of air, A, and water, W, for different inlet nozzle pressures, p_a and p_w, are displayed in Fig. 2a–c. In these 'operating diagrams', the solid lines were obtained by maintaining a constant air inlet pressure while adjusting the water flow rates and registering the corresponding air flow rates and water inlet pressures. Equivalently, the dashed lines were determined under conditions of a fixed water inlet pressure while modifying the air flow rates and recording the

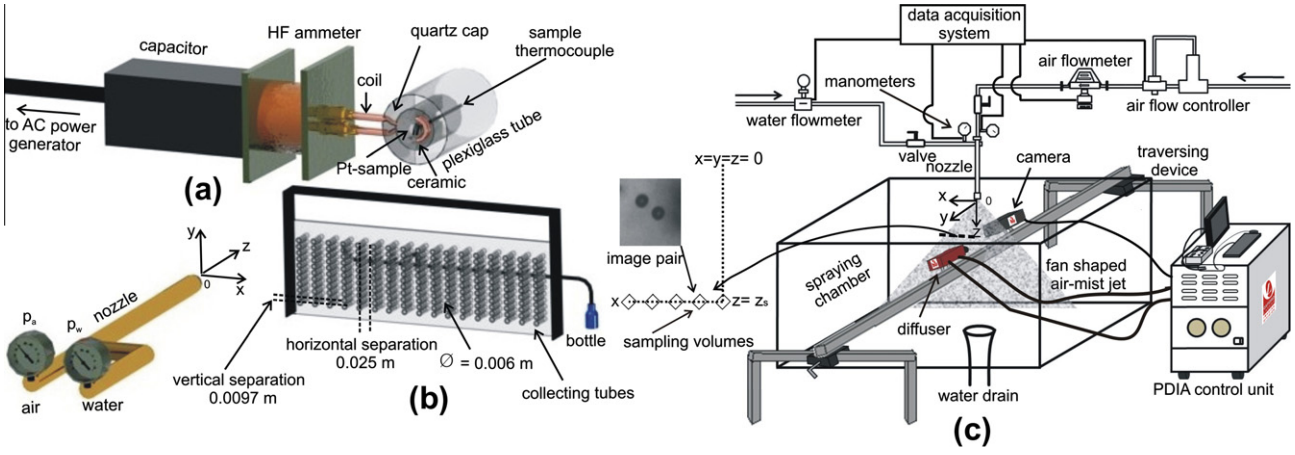

Fig. 1. Schematics of experimental apparatuses: (a) steady-state heat flux probe with HF ammeter and capacitor, (b) patternator and (c) particle droplet image analyzer, indicating the disposition of the nozzle for the different measurements and the ancillary equipment.

Table 1
Nozzles types, main expansion angles of mists and measuring positions.

Nozzle type	α (°)	z_s position (m)	x position[a] (m)	
			For $-q$ determination	For d_d and u determination
W19822	90	0.190	0, 0.06, 0.0125, 0.15, 0.16	0.00262, 0.0336, 0.0641, 0.0949, 0.1256, 0.156, 0.1873
Casterjet 1/2-6.5-90	90	0.175	0, 0.125, 0.14, 0.15, 0.165, 0.19, 0.20, 0.21	0.0012, 0.03, 0.0589, 0.0876, 0.1164, 0.1452, 0.174
Casterjet 1/2-5-60	60	0.199	0, 0.06, 0.08, 0.10, 0.125, 0.15	0.0012, 0.0293, 0.0574, 0.0855, 0.1136

[a] At $y = 0$ m.

corresponding water flow rates and air inlet pressures. Along each line of the operating diagram, the flow rates of both fluids vary at the constant inlet pressure of the specified fluid. The inlet pressure of the other fluid varies between the values corresponding to the ends of the lines for Fig. 2a or to the intersections in the case of Fig. 2b and c. For an example with the W19822 nozzle, $W = 0.041$ L/s and $p_a = 300$ kPa corresponds to $A \approx 1.4$ NL/s and $p_w \approx 305$ kPa according to Fig. 2a. From the operating diagrams, it is appreciated that there are considerable differences in the flow rates handled by the three nozzles. The dots drawn in each of them indicate the set of nozzle operating conditions investigated in the heat flux and spray parameters characterization experiments, which span a good part of the diagrams.

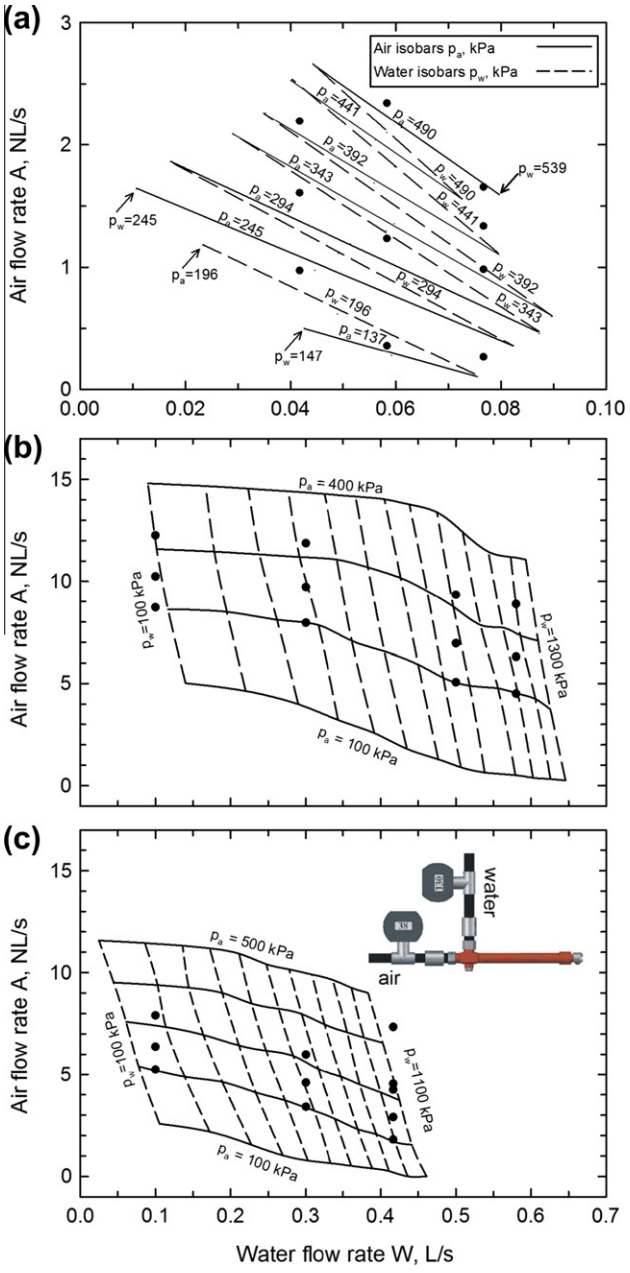

Fig. 2. Operating diagrams of nozzles: (a) W19822, (b) Casterjet 1/2-6.5-90 and (c) Casterjet 1/2-5-60, determined in the laboratory. The experimental conditions are denoted by the dots.

3. Spray parameter experimental methods and conditions

Schematics of the experimental set-ups used to measure the spray parameters are shown in Fig. 1b and c. They consist, respectively, of a patternator for measuring water impact density distributions and of a particle/droplet image analyzer (PDIA) system for acquiring and analyzing the images of fast moving droplets in dense sprays. To determine the water impact density, the nozzle was oriented horizontally, like in the high temperature experiments, as shown in Fig. 1b. In preliminary experiments the droplet size and velocity measurements were repeated with the nozzle positioned horizontally and vertically downward, and as shown in Section 4.1 the results were not significantly different. Because the vertical nozzle orientation, shown in Fig. 1c diminished splashing of water towards the diffuser and camera facilitating the use of a short distance between them, which enhances image quality, this nozzle orientation was used for most of the measurements. Also as seen in Fig. 1c, the spray parameters were determined for non-impinging free air-mists at different sampling locations along the major x-axis of the virtual impact plane; the figure displays the coordinate system and the schematic of the sampling volumes. The water and air supply system shown in Fig. 1c was essentially the same for the measurement of: $-q$, d_d and u and w, ensuring consistent flow rates for the different tests.

The PDIA system (VisiSizer N60V, Oxford Laser Ltd. Didcot, United Kingdom) schematically illustrated in Fig. 1c is a spatial multiple counting apparatus that captures a collection of instantaneous shadow images of droplets moving through small probe volumes and analyzes them in real time [30]. It employs a dual head Nd:YAG laser that sends light pulses (15 mJ at 532 nm) through a fluorescent diffuser that illuminates the region of interest from behind, while shadow images of the subjects are taken with a high resolution (4 Mpixels, 15 Hz) digital camera. The figure indicates the position of these PDIA components relative to the mist jet. Since the droplet sizes vary widely, two different lens magnifications were employed at each of the selected sampling positions given in Table 1. With these magnifications it was possible to resolve drops with diameters between 5 and 366 μm and with velocities as large as 185 m/s. The area of the field of view for both magnifications was set at 2.561×2.561 mm^2 and the depth of field for both cases was ~400 μm. Because the sampling volumes were nearly the same, all of the data were assembled together for statistical analysis. Operating in double pulse mode for simultaneous measurement of size and velocity, the laser and camera were triggered so that consecutive short pulses, lasting 4 ns, separated by a time

interval of 1.7 μs clearly captured the drops appearing in each sampling volume. The size of the drops was obtained from the analysis of images in single frames and the velocities were calculated from the displacements measured from image pairs formed by overlapping consecutive frames, and example of an image pair is included in Fig. 1c. The criteria taken into account for consideration of single drops and drop pairs were described by Minchaca et al. [30]. For each condition studied, 2000 frames (1000 at each magnification) were analyzed in real time. This number of frames sampled over 5500 drops, which ensures statistical confidence limits of 95% [31]. The nozzle conditions for the measurements are represented by the dots plotted in Fig. 2a–c.

The volume mean diameter, d_{30} (i.e., the diameter whose volume times the number of droplets, N, is equal to the volume of the entire spray) was evaluated to consider the volume of the drops associated with the impinging water volume flux, according to the following equation,

$$d_{3,0} = \left(\sum_{i=1}^{N} d_{d,i}^3 \Big/ N \right)^{1/3} \tag{5}$$

where $d_{d,i}$ is the diameter of each drop i in a sample of N droplets. Additionally, the z and x volume-weighted mean velocity components defined, respectively, as,

$$u_{z,v} = \sum_{i=1}^{N} u_{z,i} d_{d,i}^3 \Big/ \sum_{i=1}^{N} d_{d,i}^3; \quad u_{x,v} = \sum_{i=1}^{N} u_{x,i} d_{d,i}^3 \Big/ \sum_{i=1}^{N} d_{d,i}^3 \tag{6}$$

were evaluated to consider the volume of each drop i reaching the virtual impact plane with normal and tangential velocity components $u_{z,i}$ and $u_{x,i}$, respectively.

The local water impact density was assessed by measuring the volume of water, v, collected over a prescribed period of time, t, in bottles connected to tubes with a cross-section area, a, placed at positions x–y–z_s, according to the following expression,

$$w(x, y, z_s) = \frac{v}{t \cdot a \cos\theta} \tag{7}$$

where $(\cos\theta)$ is the direction cosine of the angle formed between the nozzle axis and the line connecting the center of the nozzle orifice with the center of the entrance of a given collecting tube and was introduced to consider the projected area of the collecting tubes perpendicular to the direction of motion of the drops. The diameters of the collecting tubes and their separations are given in Fig. 1b.

4. Results: mist parameters

In a recent study by some of the authors [30], the size and velocity distributions of droplets generated by Casterjet 1/2-6.5-90 and 1/2-5-60 nozzles were analyzed as a function of their operating conditions. In this work those results plus new measurements obtained for a Delavan W19822 nozzle are analyzed together with water impact density measurements to identify the fluid dynamic parameters that influence air-mist cooling and to quantify how they affect the heat extraction process. From the large number of nozzle conditions and positions included in the study (given in Fig. 2 and Table 1) only a small selection of all of the distributions and ensemble averages of the mist characteristics are presented in Sections 4.1-4.3, using some of the W19822 nozzle results to illustrate the general trends.

4.1. Distributions of droplet size, velocity and Weber number

Fig. 3a and b shows, respectively, the number frequency distributions of drop size and velocity measured at three sampling positions with a W19822 nozzle operating at the given conditions and oriented horizontally and vertically downward. It is seen that the jet orientation has little effect, on the size and on the velocity of the drops. For the internal mixing nozzles of the type used here there is strong evidence that the drops form where the two fluid streams (air and water) meet and that they are accelerated to their terminal velocities while travelling towards the nozzle exit [32,33]. Once the drops are discharged, they start to lose their momentum by interacting with the air and calculations demonstrate that for the mist jets studied, the discharge orientation does not have a significant effect on the drops motion within the trajectory lengths of interest [34], agreeing with the experimental findings of Fig. 3b. From the drops size histograms, it is also apparent that the finer and coarser drops tend to be slightly more frequent at the inner and outer regions of the mist, respectively. Different from the size distributions, which are strongly skewed to the right, the velocity distributions are nearly symmetric, exhibiting an almost normal distribution, as seen in Fig. 3b. Also in contrast to the size distributions, the velocity distribution mode (i.e., the value with the highest frequency in the distribution curve) varies with position, decreasing from the center to the edge of the mist jet. The droplets in the periphery of the mist interact more intimately with the surrounding stagnant medium, entraining air into the mist while losing their momentum. These trends are similar to those observed with the other nozzles [30].

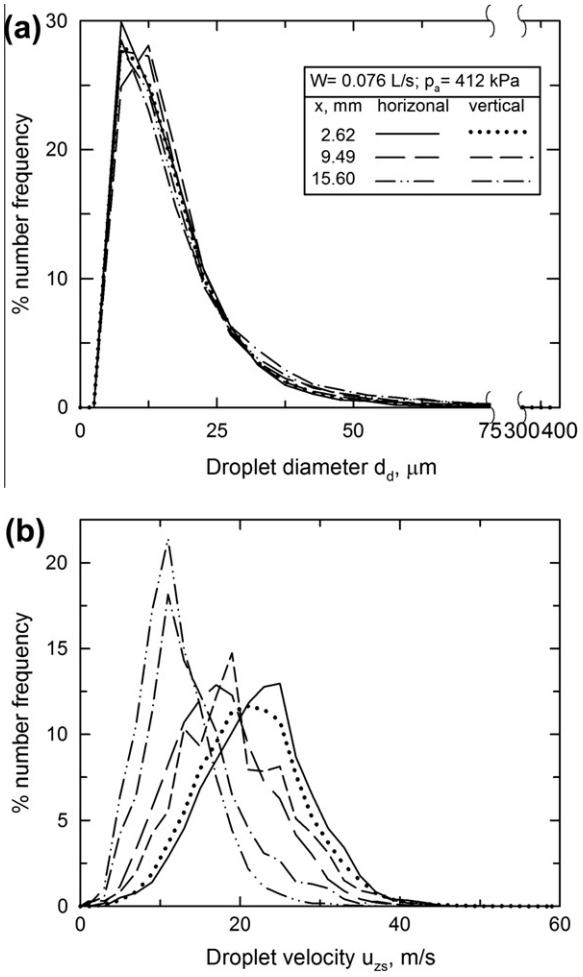

Fig. 3. (a) Droplet size and (b) droplet velocity number frequency distributions, determined at sample volumes located at the given x-positions of the major axis of the virtual impact plane. The measurements were done in mist jets oriented horizontally and vertically downward.

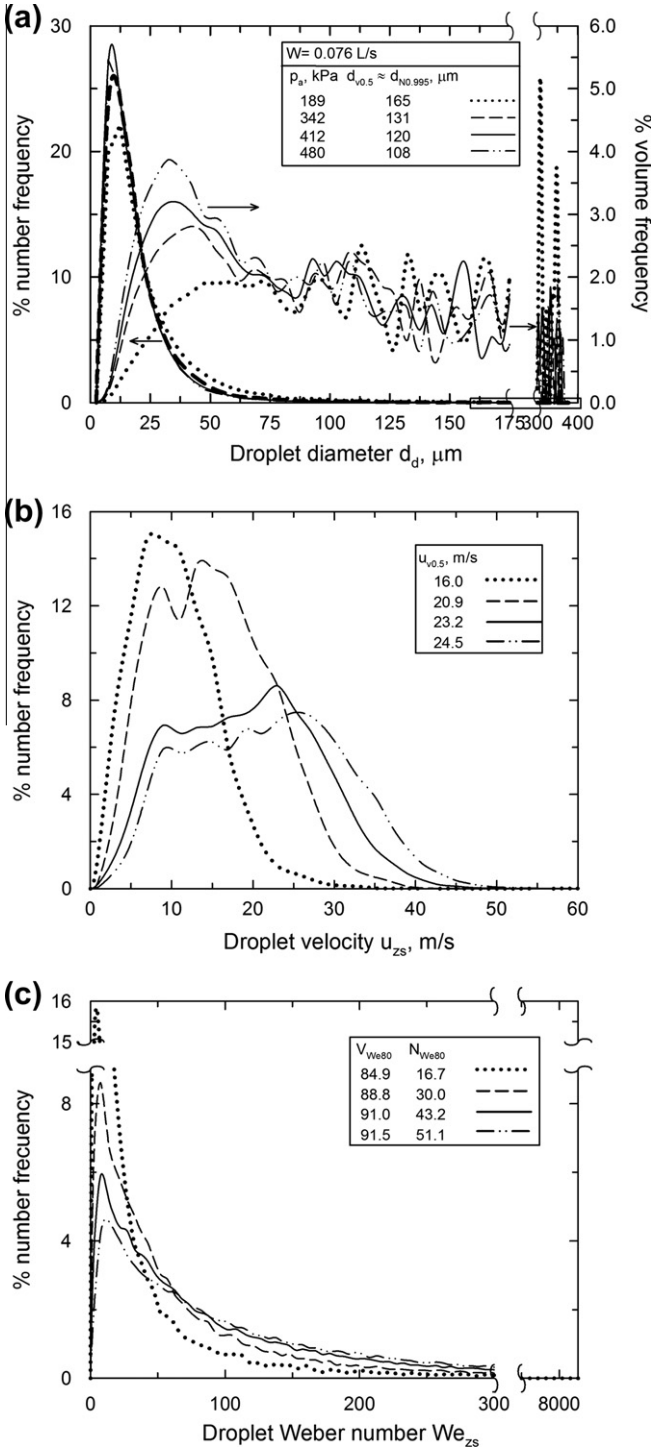

Fig. 4. Measured: (a) drop size number and volume frequency distributions, (b) drop velocity number frequency distributions and (c) drop Weber number frequency distributions, obtained with a W19822 nozzle operating at different p_a and a single W. The curve types in the different plots are according to the p_a in (a).

Fig. 4a displays droplet sizes measured with the W19822 nozzle operating at different air inlet pressures at constant $W = 0.076$ L/s. This graph shows number and volume frequency distributions for the ensemble of data measured at the seven sampling volumes centered around the x–y positions listed in Table 1. From the graph it is seen that the number frequency distributions are strongly skewed to the right. It is also apparent that increasing the air inlet pressure generates more small drops, while the frequency of larger ones decreases. In agreement with these results the volume frequency distribution curves show that the fraction of the water volume flux associated with smaller-size drops (smaller than ~50 µm) also increases as the air inlet pressure increases. As the results reported in the figure legend shows the 99.5 numeric percentile (i.e., the diameter below which 99.5% of the number of diameters are found) corresponds approximately to the volume median diameter (i.e., to the diameter, $d_{V0.5}$, which divides the sample volume exactly into halves), for all the conditions presented. Hence, the other volume half is contributed by the remaining numeric per cent of drops (i.e., by 0.5%) with sizes between ~110 and 370 µm; the thin rectangle drawn on the horizontal axis indicates schematically that the number frequency of the largest drops stays very low. As seen in the figure the volume frequency of drops larger than 75 µm fluctuated appreciably since these drops are relatively few in number but contribute greatly to the volume of water transported by the drops. Hence, small fluctuations in the number frequency of 'large' drops constitute important fluctuations in volume frequency. The results are in accordance with previous ones [30] and as pointed out highlight the need to ensure an adequate sampling of the drops to assess their statistics correctly. Thus, in conformity with ASTM guidelines [35] it was ensured that in all the measurements done the largest drop size detected made less than 1 pct of the volume of the spray flux. For all the nozzles and operating conditions investigated the number and volume frequency distributions of droplet diameter were well represented by log-normal and Nukiyama–Tanasawa distributions, respectively, [30].

Number distributions of droplet velocity are presented in Fig. 4b for the W and p_a conditions given in Fig. 4a; it should be noticed that the line types of the curves in Fig. 4b and c are consistent with those of Fig. 4a. Different from the size distributions, the velocity distributions tend to be less skewed to the right and their mode shows an appreciable increase with increasing air-atomizing pressure, suggesting that this pressure plays a higher influence in the acceleration of the drops than in the atomization of the water. The volume median velocities shown in the figure legend reveal a considerable increase in droplet velocity as the air inlet pressure increases.

As reviewed in Section 1 [8,9,15], a critical factor governing the impact and deformation mode of impinging drops is the ratio of their inertial to surface tension forces as given by the Weber number. Although, the different behaviors of drops interacting with hot surfaces have been mainly identified from observations carried out on individual drops, it can be conjectured that the interaction of a spray with a hot target will be also influenced by the We_{zs} of the drops conforming the spray. Fig. 4c shows the number frequency distributions of the droplet Weber numbers for free mists generated under different air-atomizing pressures at a constant water flow rate, and evaluated from drops measured at the virtual impact plane. For the W19822 nozzle, the figure shows that the frequency of drops with $We_{sz} \leqslant 30$ decreases as the air inlet pressure increases. The number frequency curves intersect at We_{zs} between 30 and 60 indicating that thereafter the probability of drops with higher We_{zs} increases as p_a increases. For the Casterjet nozzles, the curves cross at $We_{zs} \approx 80$ as reported elsewhere [30] and which coincidentally agrees with the critical Weber number for splashing [8]; the difference regarding the value of We_{zs} number at which the increase in p_a causes an increase in the frequency of drops with large inertia arises from the different designs and operating conditions of the W19822 and the Casterjet nozzles. The legend of Fig. 4c shows that the volume, V_{We80}, and in particular the number, N_{We80}, frequency of drops with Weber numbers greater than 80 increases greatly with increasing air inlet pressure. The increase of N_{We80} suggests that mists generated at high air inlet pressures will subject the surface to a frequent bombardment by inertially

dominated drops. The result would suggest an enhanced wet contact when the drops fall on exposed sites of a surface or a vigorous stirring or piercing of liquid films formed on the surface by precedent drops. Also, high Weber number droplets can penetrate through vapor films establishing wet contact with the surface [9,14,15]. Considering that We_{zs} increases with $u_z^2 d_d$ it is evident that the increase in droplet velocity caused by the increase in air pressure outweighs the accompanying reduction in drop size, leading to higher N_{We80} and V_{We80} at higher pressure.

In general, the effect of increasing the water flow rate at constant air inlet pressure is to increase the size of the droplets and to decrease their velocity. The final outcome of this type of operating conditions is to decrease both V_{We80} and N_{We80}, indicating a smaller volume of the liquid and a smaller frequency of the drops that would cause intense impingement; results regarding this behavior of the mists have been presented elsewhere [30].

4.2. Spatial distribution of volume mean diameter and volume weighted mean velocity

As mentioned in Section 3, the size and velocity of the drops reaching the virtual impact plane were measured by PDIA at several locations across the major x-axis of the cross-section of the fan-shaped mist jet, at $z = z_s$. Fig. 5 shows the spatial distribution of the volume mean diameter obtained with the W19822 nozzle operating at air-atomizing pressures of 189, 342, 412 and 480 kPa with a constant water flow rate of 0.076 L/s. The profiles displayed in the figure indicate that at constant water flow rate, the increase in air inlet pressure led to the formation of finer drops, due to the higher shearing work per unit volume done by the air to the drops formed by the inlet water splattering over a deflector surface located just up-stream of the mixing chamber of the nozzle. For these internal mixing air–water nozzle designs, illustrated in Fig. 1, the intersection of the axially moving stream of air with the cross-axial water stream results in a swirling motion of the drops, which causes the larger drops to move in the periphery of the mixing chamber and exit through the outermost positions of the orifice. This type of discharge from the nozzle orifice generates finer drops at the inner positions of the mist jet and coarser drops closer to the edges, as quantified in Fig. 5.

Profiles of the normal and tangential – in relation to the virtual impact plane – volume-weighted mean velocity components of the drops reaching the surface are presented in Fig. 6a and b, respectively. These figures reveal that at constant W, the increase in the air-atomizing pressure causes substantial increases in both velocity components of the drops. Fig. 6a shows that the z-velocity component of the droplets diminishes from the center to the edge of the air-mist jet, exhibiting a nearly bell-shaped profile. On the other hand as expected, Fig. 6b shows that the x-velocity component is zero at the center due to symmetry, and increases towards the far edge of the mist cross-section, showing a maximum before it. These results suggest that increasing air inlet pressure would cause a more vigorous impingement of the drops on a surface as a result of larger normal drop velocities, particularly in the central zone of the footprint, and also an enhanced renewal of liquid on the surface towards the periphery of the footprint, due to larger tangential velocity components.

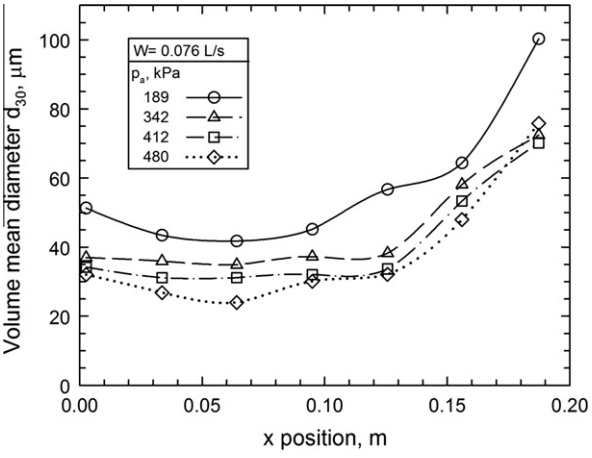

Fig. 5. Variation of droplet volume mean diameter across the major axis of the mist cross-section at $z = z_s$, for the W19822 nozzle operating at different p_a and constant W.

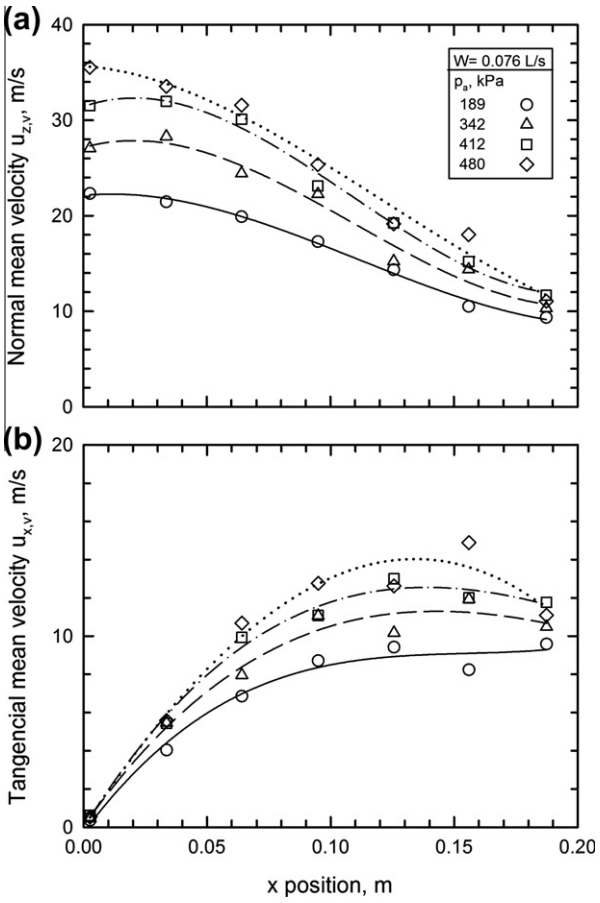

Fig. 6. Variation of: (a) normal and (b) tangential volume weighed mean velocity components across the major axis of virtual mist footprints of the W19822 nozzle, for different air-atomizing pressures and a constant water flow rate.

The trends in the distributions of d_{30}, $u_{x,v}$ and $u_{z,v}$ obtained with the W19822 nozzle are similar to those reported previously for the Casterjet nozzles [30].

4.3. Measured local impact water flux

The water impact flux pattern was determined for the 33 operating conditions indicated by the dots in Fig. 2. Examples of the distributions are shown in Fig. 7a and b for a single water flow rate and two air inlet pressures. As seen in the plots, the flat-fan nozzle generated footprints with a nearly symmetric bimodal distribution of the water flux. This type of distribution was common for all the nozzles and conditions studied and the small variation of w between the maxima permits its representation through an obelisk distribution [4,26]. To evaluate the accuracy of the water sampling

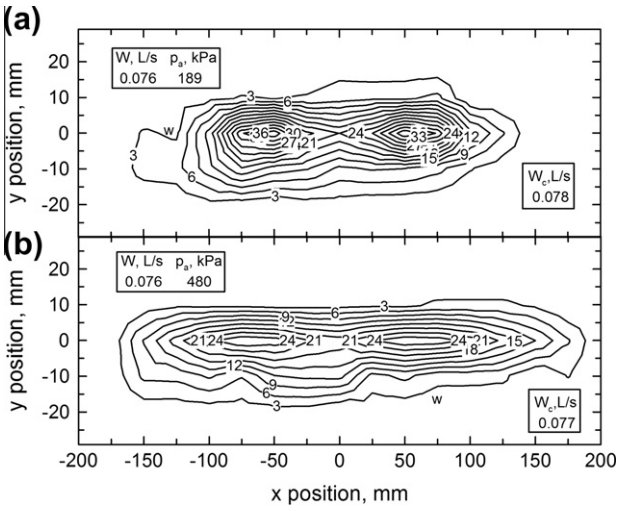

Fig. 7. Water impact density maps for a constant water flow rate and two air inlet pressures with a W19822 nozzle.

achieved with the patternator, water flow rates W_c were estimated by numerical integration of w over the footprint area and compared against the measured value W for each of the conditions studied. As can be appreciated from the legends in Fig. 7, the W_c values were in general very close to the measured ones; only in few cases was the error as large as ±10%. From the plots, it is observed that the increase in p_a caused a redistribution of the local w, by decreasing the maximum w values and increasing the footprint area, specifically by extending the major axis (width) of the footprint. As reported elsewhere [36], the effect of increasing W at constant p_a was to increase the local w.

5. Results: heat transfer

Like the air-mist fluid-dynamic parameters presented in Section 4, steady-state mist heat fluxes were measured for the three nozzles under the operating conditions given in Fig. 2 and at the positions listed in Table 1. This range of conditions covers the wide interval of local spray parameters that give rise to the enormous set of combinations that arise in practical spray cooling situations of relevance to metallurgical processes. The spray parameters varied within the following ranges: w from 2 to 106 L/m^2 s; $u_{z,v}$ from 9.3 to 45.8 m/s and d_{30} from 19 to 119 μm. The surface temperatures ranged from ~550 to 1200 °C. Because of the large number of conditions investigated, only a selected sample of results is presented to illustrate general trends and to discuss how the spray cooling intensity varied as a function of nozzle operating conditions and spray parameters. The complete set of heat fluxes and associated heat transfer coefficients obtained were correlated as a function of the spray parameters and surface temperature from ~750 to 1200 °C. Finally, heat transfer coefficients obtained by the steady-state method were compared with transient measurements [26] for the same nozzle conditions.

5.1. Effect of operating conditions on the boiling curves

Fig. 8a–d shows plots of heat flux versus surface temperature measured at different x positions using a W19822 nozzle operating with a water flow rate of 0.076 L/s and air inlet pressures of 189, 342, 412 and 480 kPa. The boiling heat flux values plotted in the figures correspond exclusively to the boiling convection component, $-q$, because the radiation contribution was subtracted, as explained in Section 2. The values plotted in the figures correspond to averages of at least two repetitions involving thermal loops from 600–1200–600 °C and/or to descending paths from 1200 to 600 °C. The error bars on the curves are quite small, which means that the results exhibited good reproducibility, and that the boiling hysteresis discussed in [1] was absent in the temperature range of 550–1200 °C.

The boiling curves at the lowest air inlet pressure, 189 kPa, occurred entirely in the stable film boiling regime, except for the condition with a larger w, shown in Fig. 8b. For this and the rest of the conditions shown in the plots of Fig. 8, cooling took place in both the stable film-boiling regime and the upper part of the transition boiling regime. The Leidenfrost temperatures, T_L, shown in the figure appear between 650 °C and 1000 °C. In the stable film boiling regime, the curves show a gentle decrease in heat flux with decreasing temperature, while in the transition boiling regime the trend is opposite and with a steeper slope. The largest Leidenfrost temperatures seem to be associated with the largest w and $u_{z,v}$, such as shown in Fig. 8b and in one case in Fig. 8a. This indicates that large local mist momentum flux (product of w and $u_{z,v}$) increases the chance of physical contact of the liquid with the surface at higher T_w. On the other hand, the opposite behavior occurs for the lowest w and/or for the lowest $u_{z,v}$, for which the boiling curves indicate lower T_L or even stable film boiling only, as observed in Fig. 8a, c and d. These findings explain the observation of Sengupta et al. [3] that the Leidenfrost temperature found in secondary cooling is lower for the low-momentum water flows used in aluminum DC-casting than for the high-momentum water spray used in the steel continuous-casting process. Thus, the effect of temperature on the boiling heat extraction depends greatly on the fluid dynamic parameters of the mist.

The legends of Fig. 8a–d show that the conditions of the current study involved w, d_{30} and $u_{z,v}$ that changed over wide ranges. A feature that is immediately evident from the plots is the increase in heat flux with increasing p_a, at constant W. This rise in $-q$ must be the result of an enhanced interaction of the drops with the hot surface, which must have arisen from the changes experienced by the spray parameters. From the legends, it is evident that the three spray parameters changed with p_a. As p_a increased, w remained constant or decreased in the central region ($x = 0$ to 0.06 m) while it increased in the outer regions (e.g., at $x = 0.125$ and 0.160 m). On the other hand, d_{30} and $u_{z,v}$ consistently grow smaller and larger, respectively. Thus, the increase in $-q$ with p_a most likely stemmed from the increase in $u_{z,v}$, as drops with larger inertia were able to spread widely over the surface, break into several secondary drops and move closer to the surface to extract more heat. Furthermore, primary drops with a large inertia could also strongly agitate the liquid and vapor films already present on the surface, and thus favor higher heat transfer. The reduction in drop size then could be beneficial for increasing the heat flux by providing a larger specific surface area.

Fig. 9a–c presents selected results where only one spray parameter changed appreciably in relation to the other two. In Fig. 9a, the results of two experiments involving similar values of w and d_{30} (varying by a factor of 1.18 and 1.03, respectively) and an important difference in $u_{z,v}$ (varying by a factor of 1.65) reveal that this parameter has a substantial influence on boiling convection heat flux in the stable film boiling regime, but that its influence is only minor in the transition boiling regime. The effect of the droplet velocity is important even at the relatively high w of the conditions in this figure. The influence of the water impact density has been isolated in Fig. 9b, where the differences in d_{30} and $u_{z,v}$ are small (varying by a factor of 1.01 and 1.05, respectively) relative to those of w (varying by a factor of 1.52). From the figure it is seen that $-q$ increases greatly with increasing w and the plot suggests that for high w and $u_{z,v}$ values the transition boiling regime start at high temperatures, even the critical heat flux, CHF, appeared within

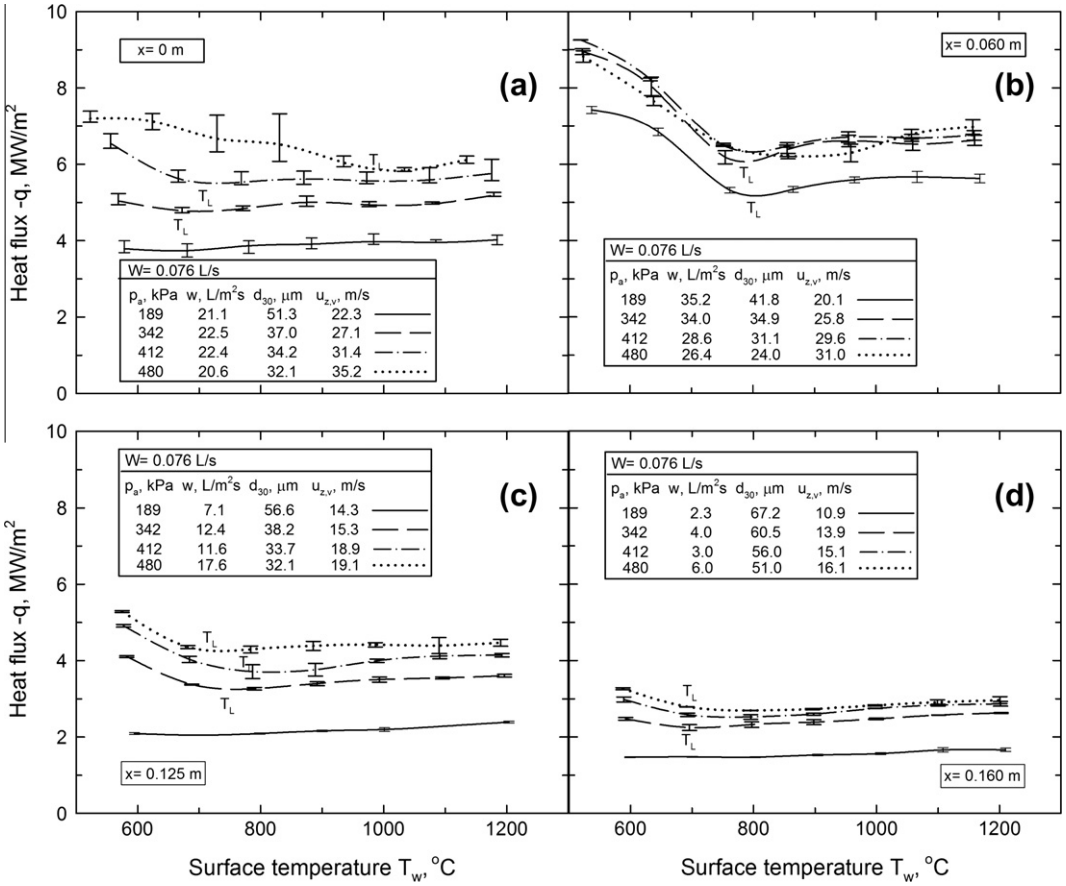

Fig. 8. Measured boiling curves for $W = 0.076$ L/s and different atomizing pressures and x-positions obtained with a W19822 nozzle.

the temperature range studied. In Fig. 9c the values of d_{30} exhibit larger differences (varying by a factor of 2.18) than the values of w and $u_{z,v}$ (varying by a factor of 1.12 and 1.13, respectively) thus, it seems that since the boiling curves overlap in the stable film and transition boiling regimes d_{30} does not affect the heat extraction by the mist. For completeness the volume weighed mean of the tangential velocity component was included in the legends of Figs. 8 and 9.

5.2. Heat flux and heat transfer coefficient correlations

The behaviors of the boiling curves presented in Figs. 8 and 9 suggest that the local spray parameters, particularly w and $u_{z,v}$, together with the surface temperature govern the intensity of the heat flux extracted from the surface of a probe specimen, placed at different positions with respect to the nozzle orifice. However, situations like those in Fig. 9 where one mist parameter varied appreciably while the other two exhibited smaller differences were too rare to quantify the effect of the individual mist parameters on $-q$. Thus, the lumped set of $-q$ values for T_w between 750 °C and 1200 °C were fitted, using the least square method, as a function of the spray parameters and surface temperature, obtaining the following power law expression,

$$-q = 0.307 w^{0.319} u_{z,v}^{0.317} T_w^{0.144} d_{30}^{-0.036} \quad (8)$$

The correlation coefficient of the data was 0.95 and the standard error was 1.156 MW/m^2. A comparison between the measured and fitted heat fluxes is shown in Fig. 10, where 94% of the 506 results fell within ±25% of the correlation. The closeness of the exponents on w and $u_{z,v}$ suggests that $-q$ is a function of their product, which represents the momentum flux on the impact surface. Additionally, the correlation indicates that the boiling heat flux also increases with T_w and is almost unaffected by d_{30}. In the range of 750–1200 °C, 6% of the measured heat fluxes fell in the transition regime but removal of this data did not affect the quality of the correlation so they were retained.

Next, the following correlation to predict the heat transfer coefficient was generated, via the same method,

$$h = 379.93 w^{0.318} u_{z,v}^{0.330} T_w^{-0.895} d_{30}^{-0.024} \quad (9)$$

where the exponents for w, $u_{z,v}$ and d_{30} are similar to those appearing in Eq. (8) but T_w plays a more significant role and indicates that in the film boiling regime, h decreases with increasing surface temperature. The correlation coefficient and standard error were 0.95 and 1.156 kW/m^2 C, respectively. A comparison between the measured and fitted heat transfer coefficients is shown in Fig. 11, where 96% of the results fell within ±25% of the correlation.

5.3. Comparison between steady-state and transient measured heat transfer coefficients

Studies of spray cooling in systems of metallurgical interest aim to employ laboratory spraying and thermal conditions similar to those found in actual processes. However, little attention has been given to understand how the thermal history of the sample surface affects the heat extraction results. Previous heat transfer correlations have been generally obtained from transient experiments [22,28]. Specifically, the surface of a hot test-specimen is sprayed and its temperature-time history is recorded simultaneously at specific locations near the surface while it cools freely, i.e., without heat sources such as latent heat that greatly affects commercial

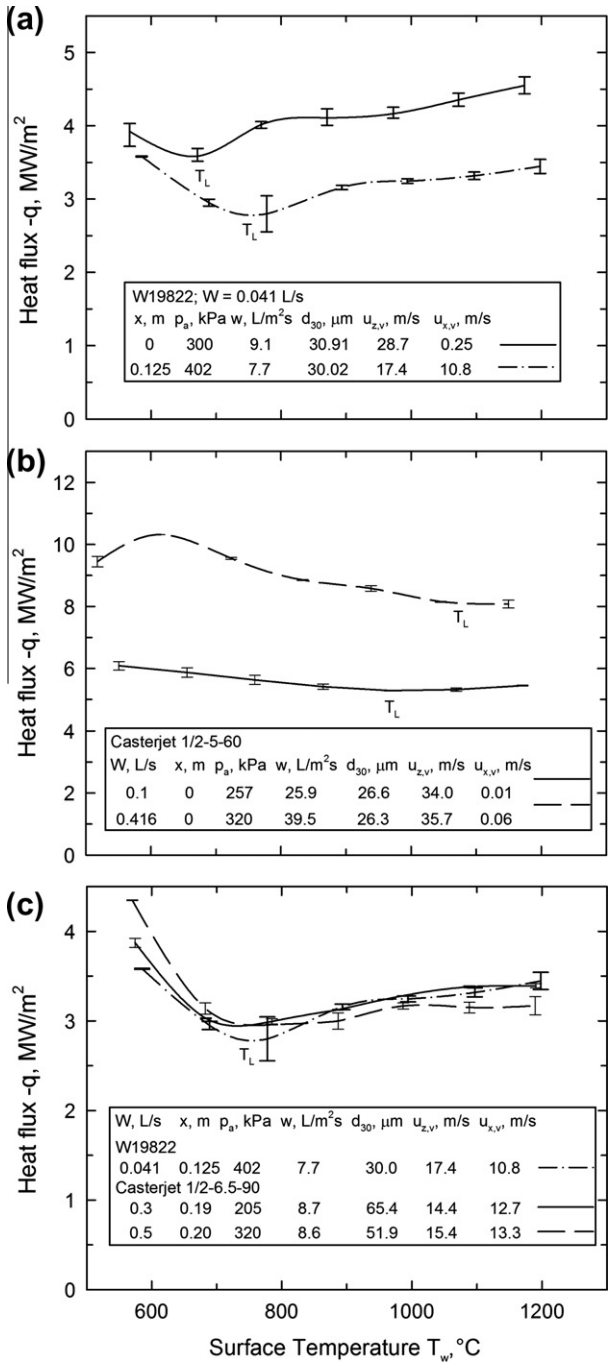

Fig. 9. Measured boiling curves showing the influence of different spray parameters: (a) effect of drop velocity, (b) effect of water impact density and (c) effect of droplet size.

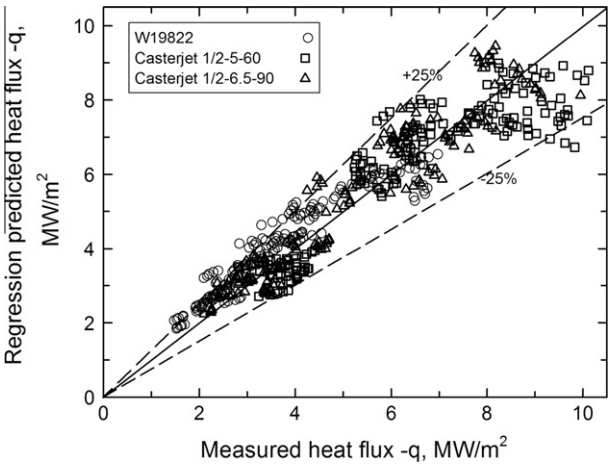

Fig. 10. Comparison between measured and correlation-calculated heat fluxes for all nozzles and conditions (506 results) from 750 to 1200 °C.

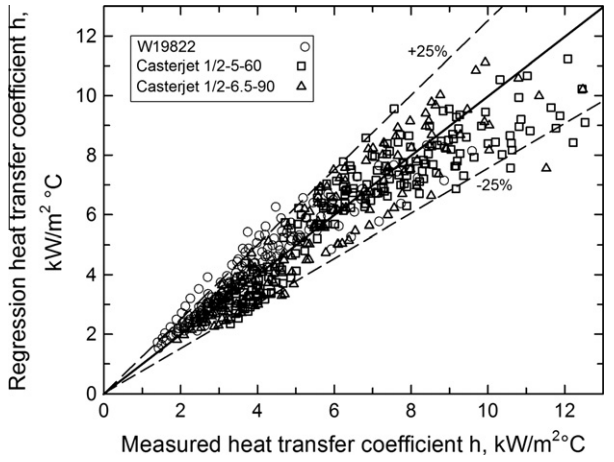

Fig. 11. Comparison between measured and correlation-calculated heat transfer coefficients for all nozzles and conditions (506 results) from 750 to 1200 °C.

casting processes. Estimation of T_w and h at the active boundary is done through the inverse solution of the transient heat conduction problem.

The thermal history of the sample in unsteady-state experiments differs greatly from that found in steady-state ones. In the transient test, the wall temperature T_w changes continuously as heat is extracted by the impinging drops while in the steady experiments, it remains constant. Thus, the interaction times of the drops with the surface at a particular temperature are much larger in steady- than in unsteady-state heat transfer experiments. Only few comparisons of the heat flux extracted under both types of techniques have been reported. Ishigai et al. [37] and Olden et al. [38] found reasonably similar results between steady- and unsteady-state experiments in the stable film boiling regime and in the transition boiling regime, respectively. In the first study [37] the surface temperatures used were as high as 1000 °C but the impinging velocities where low $\leqslant$3.5 m/s, while in the second study [38] the wall temperature ranged from 200 to 500 °C and $w = 2$ L/m^2 s. These conditions are far away from those of interest, which involve intense cooling of highly superheated surfaces, as is the case of metallurgical processes and emergency cooling systems of nuclear reactors. Until the present study, the difficulties in using steady-state techniques with intense heat extraction banned the possibility of comparing results of the two methods.

Comparing heat flux results from steady and unsteady conditions provides important insight into the application of laboratory measurements to industrial processes. Transient experiments reported elsewhere by some of the investigators [26,28] cover similar spraying conditions (W, p_a) as in the present work, but with a 304-SS sample instead of Pt. A clean Pt surface in air has a hydrophilic nature similar to oxidized metal surfaces [39], so should have a similar dynamic wetting behavior. The thermal diffusivity of Pt is about four times larger than that of 304-SS for 700–1200 °C temperatures, but this does not matter unless internal heat conduction in the sample is important.

Fig. 12 shows the variations of the heat transfer coefficient as a function of the water impact flux for two temperatures,

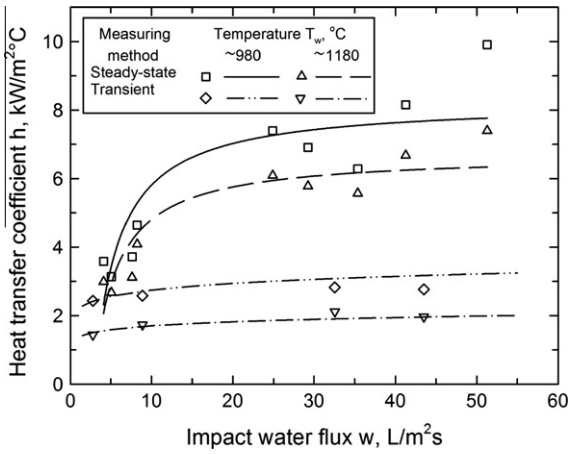

Fig. 12. Comparison between steady-state and transient measurements of heat transfer coefficients as a function of w for two T_w, obtained with a Casterjet 1/2-6.5-90 nozzle with p_a and W ~250 kPa and ~0.5 L/s, respectively.

determined by the steady-state method of the present work and by the transient technique reported elsewhere [28]. It is seen that in agreement with the findings of Ishigai et al. [37] at low water impact densities, $w < 5$ L/m^2 s, both techniques led to similar results. Based on the results of Bernardin et al. [14] and Chen and Hsu [40] it can be thought that since the temperatures are high enough, 980 °C and 1180 °C, and the droplet number flux sufficiently low then the transient system has sufficient enthalpy to recover the temperature of the surface during the time elapse between consecutive drops impingements, thus approaching the steady-state experimental conditions. For w between 5 and 20 L/m^2 s the h measured under steady state conditions increases steeply, very different from what is observed for transient conditions. This behavior suggests that under constant supply of heat to the surface the heat extraction is controlled by the local water flux supplied to the surface. In transient conditions with the lower-conductivity material, however, the rate limiting step for surface heat extraction appears to be the supply of heat conducted from the interior of the sample and its limited sensible enthalpy. In the steady state experiments, further increase in w beyond 20 L/m^2 s causes only an asymptotic increase in h. This suggests that an excessive supply of water to the surface leads a thick water film that hinders evaporation from its free surface and contact of new water with the target surface.

The large differences between the magnitudes of the heat fluxes and heat transfer coefficients measured by steady-state and transient methods, under similar spraying conditions – for $w \geqslant 5$ L/m^2 s – point out the important role that the target thermal history and its internal heat transfer plays on the heat extraction from the surface. The significance of the thermal trajectory on the heat extraction outcome was also observed in steady-state experiments, when following different thermal paths while passing through the nucleate and transition boiling regimes [1]. These behaviors emphasize the need to consider the influence of thermal history on the phenomena involved in mist cooling, both of the surface and interior of the sample, in order to enable accurate laboratory simulation of the cooling conditions that take place in industrial processes. Further investigations are underway to evaluate transient and steady-state methods in more detail.

6. Summary and conclusions

A novel steady-state method based on induction heating was applied in this work to study the influence of air-mist characteristics on the heat extracted by boiling convection from the surface of a Pt-disk at highly-superheated surface temperatures, ranging from 550 °C to 1200 °C. Three typical commercial air-mist nozzles with fan-shaped discharge were positioned at their usual setback distance from the hot surface, and investigated over a wide range of water flow rates, W, and air inlet pressures, p_a. Measurements for many different test conditions were combined to study the independent effects of droplet diameter, droplet velocity and water impact density. A particle/droplet image analyzer was used to determine the first two parameters by collecting statistically meaningful samples of over 6000 drops and the water impact density was measured employing a patternator. The averages of the water-droplet parameters in the free air mist varied within the intervals: d_{30} from 19 to 119 μm, $u_{z,v}$ from 9.3 to 45.8 m/s and w from 2 to 106 L/m^2 s.

Analysis of the droplet size distributions revealed that the smaller drops (<100–170 μm, depending on the nozzle and operating conditions) were the most numerous (99.5%) but comprised only half of the volume. Hence, a very small numeric percentage (0.5%) of large drops with sizes between that interval and 370 μm contributed the other 50% of the volume flux reaching the hot surface. For constant W, increasing p_a generated smaller and faster moving droplets, where the increase in velocity dominated over the decrease in size, to increase the number and volume frequency of droplets with $We_{zs} > 80$. It can be thought that the resulting increased inertia and improved contact of the drops with the surface during impingement caused the boiling convective heat flux $-q$ to increase with increasing p_a for given T_w and W values. A correlation to predict the boiling convection heat flux within the stable film boiling regime was obtained from a best fit of the results, as: $-q = 0.307 w^{0.319} u_{z,v}^{0.317} T_w^{0.144} d_{30}^{-0.036}$. This relation shows that the most important spray/mist parameters are the water flux and the droplet velocity, and that the other influential parameter is the surface temperature. The relative importance of the parameters was confirmed by results where their individual effects could be isolated.

A comparison of the results from steady-state and transient experiments reveals that for $w > 5$ L/m^2 s, the steady-state method gives considerably larger boiling heat fluxes. The rapid increase in h with w from 5 to 20 L/m^2 s under steady-state conditions suggests that the heat extraction is controlled by the supply of water to the surface. In transient experiments, the rate limiting step for heat extraction appears to be the supply of heat conducted from the interior of the sample. These results clearly show the need to understand the phenomena involved in mist/spray cooling, in order to select laboratory cooling conditions that simulate appropriately those found in industrial processes. The steady-state induction-heating-based method presented and applied in this work enables fundamental research into mist/spray cooling, especially of highly superheated surfaces subjected to intense spraying conditions.

Acknowledgements

We are grateful to the National Council of Science and Technology of Mexico (CONACYT) and the National Science Foundation (US) for financial support through Grants Nos. 57836 and CMMI-0900138, respectively, and also to the Continuous Casting Consortium at the University of Illinois. CAHB/JIMM and XZ wish to thank CONACYT and the CCC, respectively, for their scholarship grants.

References

[1] C.A. Hernández B., A.H. Castillejos E., F.A. Acosta G., X. Zhou, B.G. Thomas, Measurement of heat flux in dense air-mist cooling: Part I. A novel steady-state technique, Experimental Thermal and Fluid Science, accepted for publication.
[2] Stahl. Steel in Figures, World Crude Steel Production, 2011. <http://www.stahl-online.de/english/>.

[3] J. Sengupta, B.G. Thomas, M.A. Wells, The use of water cooling during continuous casting of steel and aluminum alloys, Metallurgical and Materials Transactions B 36 (1) (2005) 187–204.
[4] J.E. Camporredondo S., A.H. Castillejos E., F.A. Acosta G., E.P. Gutiérrez M., M.A. Herrera G., Analysis of thin slab casting by the compact-strip process: Part I. Heat transfer and solidification, Metallurgical and Materials Transactions B 35 (3) (2004) 541–559.
[5] S.G. Hibbins, J.K. Brimacombe, Characterization of heat transfer in the secondary cooling system of a continuous slab caster, ISS Transactions 3 (1983) 77–89.
[6] C.O. Pedersen, An experimental study of the dynamic behavior and heat transfer characteristics of water droplets impinging upon a heated surface, International Journal of Heat and Mass Transfer 13 (2) (1970) 369–379.
[7] J.D. Bernardin, I. Mudawar, Film boiling heat transfer of droplet streams and sprays, International Journal of Heat and Mass Transfer 40 (11) (1997) 2579–2593.
[8] L.H.J. Wachters, N.A. Westerling, The heat transfer from a hot wall to impinging water drops in the spheroidal state, Chemical Engineering Science 21 (11) (1966) 1047–1056.
[9] M. Rein, Interactions between drops and hot surfaces, in: M. Rein (Ed.), Drop-Surface Interactions, Springer, Wien New York, Udine, 2002, pp. 185–217.
[10] A.L.N. Moreira, A.S. Moita, M.R. Panão, Advances and challenges in explaining fuel spray impingement: how much of single droplet impact research is useful?, Progress in Energy and Combustion Science 36 (5) (2010) 554–580
[11] A.L.N. Moreira, M.R.O. Panão, Spray-wall impact, in: N. Ashgriz (Ed.), Handbook of Atomization and Sprays: Theory and Applications, Springer, New York, 2011, pp. 441–455.
[12] M.R.O. Panão, A.L.N. Moreira, Experimental study of the flow regimes resulting from the impact of an intermittent gasoline spray, Experiments in Fluids 37 (6) (2004) 834–855.
[13] S.W. Park, C.S. Lee, Macroscopic and microscopic characteristics of a fuel spray impinged on the wall, Experiments in Fluids 37 (6) (2004) 745–762.
[14] J.D. Bernardin, C.J. Stebbins, I. Mudawar, Mapping of impact and heat transfer regimes of water drops impinging on a polished surface, International Journal of Heat and Mass Transfer 40 (2) (1997) 247–267.
[15] R.J. Issa, S.C. Yao, Numerical model for spray-wall impaction and heat transfer at atmospheric conditions, Journal of Thermophysics and Heat Transfer 19 (4) (2005) 441–447.
[16] A.H. Lefebvre, Atomization and Sprays, CRC Press, FL, 1989. pp. 106–153.
[17] G.G. Nasr, A.J. Yule, L. Bendig, Industrial Sprays and Atomization – Design, Analysis and Applications, Springer, Great Britain, 2002. pp. 7–32.
[18] K.J. Choi, S.C. Yao, Mechanisms of film boiling heat transfer of normally impacting spray, International Journal of Heat and Mass Transfer 30 (2) (1987) 311–318.
[19] G.P. Celata, M. Cumo, C. Lombardo, A. Mariani, L. Saraceno, Experimental result on rewetting of hot surfaces by droplet impingement, Experimental Thermal and Fluid Science 29 (3) (2005) 275–285.
[20] J.K. Brimacombe, P.K. Agarwal, L.A. Baptista, S. Hibbins, B. Prabhakar, Spray cooling in the continuous casting of steel, in: National Open Hearth and Basic Oxygen Steel Division of AIME (Ed.), Steelmaking Proceedings, NOH-BOS Conference, ISS-AIME, Washington, 1980, pp. 235–252.
[21] R.-H. Chen, L.C. Chow, J.E. Navedo, Effects of spray characteristics on critical heat flux in subcooled water spray cooling, International Journal of Heat and Mass Transfer 45 (19) (2002) 4033–4043.
[22] M. Ciofalo, I. Di Piazza, V. Brucato, Investigation of the cooling of hot walls by liquid water sprays, International Journal of Heat and Mass Transfer 42 (7) (1999) 1157–1175.
[23] J. Schmidt, H. Boye, Influence of velocity and size of the droplets on the heat transfer in spray cooling, Chemical Engineering Technology 24 (3) (2001) 255–260.
[24] H. Fujimoto, N. Hatta, H. Asakawa, T. Hashimoto, Predictable modelling of heat transfer coefficient between spraying water and a hot surface above the Leidenfrost temperature, ISIJ International 37 (5) (1997) 492–497.
[25] L. Bendig, M. Raudensky, J. Horsky, Spray parameters and heat transfer coefficients of spray nozzles for continuous casting, in: Proceedings of the Seventy Eight Steelmaking Conference, Iron and Steel Society, Nashville, TN, 1995, pp. 391–398.
[26] J.J. Montes R., A.H. Castillejos E., F.A. Acosta G., E.P. Gutiérrez M., M.A. Herrera G., Effect of the operating conditions of air-mists nozzles on the thermal evolution of continuously cast thin slabs, Canadian Metallurgical Quarterly 47 (2) (2008) 187–204.
[27] M.S. Jenkins, S.R. Story, R.H. David, Defining air-mist nozzle operating conditions for optimum spray cooling performance, in: Proceedings of the Nineteenth Australasian Chemical Engineering Conference, September 12–20, Institute of Engineers, Newcastle, New South Wales, Australia, 1991, pp. 161–169.
[28] A.H. Castillejos E., F.A. Acosta G., M.A. Herrera, I. Hernández C., E.P. Gutiérrez M., Practical productivity gains – towards a better understanding of air-mist cooling in thin slab continuous casting, in: R.I.L. Guthrie (Ed.), Proceeding of the Third International Congress of Steelmaking, Association of Iron and Steel Technology, Charlotte, NC, 2005, pp. 881–890.
[29] M.R.O. Panão, A.L.N. Moreira, Heat transfer correlation for intermittent spray impingement: a dynamic approach, International Journal of Thermal Sciences 48 (10) (2009) 1853–1862.
[30] J.I. Minchaca M., A.H. Castillejos E., F.A. Acosta G., Size and velocity characteristics of droplets generated by thin steel slab continuous casting secondary cooling air-mist nozzles, Metallurgical and Materials Transactions B 42 (3) (2011) 500–515.
[31] I.G. Bowen, G.P. Davies, Particle Size Distribution and the Estimation of Sauter Mean Diameter, Technical Report ICT 28, Shell Research Ltd., London, 1951.
[32] I. Hernández C., F.A. Acosta G., A.H. Castillejos E., J.I. Minchaca M., The fluid dynamics of secondary cooling air-mist jets, Metallurgical and Materials Transactions B 39 (5) (2008) 746–763.
[33] J.I. Minchaca M., A.H. Castillejos E., F.A. Acosta G., S. Murphy, Fluid dynamics of thin steel slab continuous casting secondary cooling zone air mists, in: M. Herrmann (Ed.), Proceedings of the ILASS-Americas 22nd Annual Conference on Liquid Atomization and Spray Systems, International Liquid Atomization and Spray Systems – Americas, Cincinnati, OH, 2010. Paper 143.
[34] J.I. Minchaca M., Ph.D. Thesis, CINVESTAV – Unidad Saltillo, Coahuila, México, 2012, in press.
[35] ASTM Standard Practice for Determining Data Criteria and Processing for Liquid Drop Size Analysis, Designation E799–92 (Reapproved 1998), 1998.
[36] C.A. Hernández B., Ph.D. Thesis, CINVESTAV – Unidad Saltillo, Coahuila, México, 2012, in press.
[37] S. Ishigai, S. Nakanishi, T. Ochi, Boiling heat transfer for a plane water jet impinging on a hot surface, in: Proceedings of the Sixth International Heat Transfer Conf, Hemisphere Pub. Corp., Toronto, Canada, 1978, pp. 445–450.
[38] V. Olden, M. Raudensky, K. Onsrud, W. Hummel, Water spray cooling of stainless and C–Mn steel, Steel Research 69 (6) (1998) 240–246.
[39] M.L. White, The wetting of gold surfaces by water, The Journal of Physical Chemistry 68 (10) (1964) 3083–3085.
[40] J.C. Chen, K.K. Hsu, Heat transfer during liquid contact on superheated surfaces, Journal of Heat Transfer 117 (3) (1995) 693–697.